Assessment of Tissue Damage due to Mechanical Stresses

Smita De, Jacob Rosen, Aylon Dagan, Blake Hannaford, Paul Swanson and Mika Sinanan

The International Journal of Robotics Research 2007; 26; 1159
DOI: 10.1177/0278364907082847

Assessment of Tissue Damage due to Mechanical Stresses

Smita De
Jacob Rosen
Aylon Dagan
Blake Hannaford

BioRobotics Laboratory, Department of Bioengineering
University of Washington Box 352500, Seattle,
WA 98195-2500, USA
{sd6, rosen}@u.washington.edu, ldagan@gmail.com,
blake@ee.washington.edu

Paul Swanson

Department of Anatomic Pathology
University of Washington Box 352500, Seattle,
WA 98195-2500, USA
ps3@u.washington.edu

Mika Sinanan

Department of Surgery,
University of Washington Box 352500, Seattle,
WA 98195-2500, USA
mssurg@u.washington.edu

Abstract

While there are many benefits to minimally invasive surgery (MIS), force feedback or touch sensation is limited in the currently available MIS tools, such as surgical robots, creating the potential for excessive force application during surgery and unintended tissue injury. The goal of this work was to develop a methodology with which to identify stress magnitudes and durations that can be safely applied with a MIS grasper to different tissues, potentially improving MIS device design and reducing potentially adverse clinically relevant consequences. Using the porcine model, stresses typically applied in MIS were applied to liver, ureter and small bowel using a motorized endoscopic grasper. Acute indicators of tissue damage including cellular death and infiltration of inflammatory cells were measured using histological and image analysis techniques. Finite element analysis was used to identify approximate stress distributions experienced by the tissues. Parameters used in these finite element models specifically reflected the properties of liver, which served as an initial proxy for all tissues, as stress distributions rather than absolute values were desired. Local regions predicted to have uniform stress by the computational models were mapped to and analyzed in the tissue samples for acute damage. Analysis of variance (ANOVA) and post-hoc analyses were used to detect stress magnitudes and durations that caused significantly increased tissue damage with the goal to ultimately identify safe stress 'thresholds' during grasping of the studied tissues. Preliminary data suggests a graded non-linear response between applied stress magnitude and apoptosis in liver and small bowel as well as neutrophil infiltration in the small bowel. The ureter appeared to be more resistant to injury at the tested stress levels. By identifying stress magnitudes and durations within the range of grasping loads applied in MIS, it may be possible for researchers to create a 'smart' surgical robot that can guide a surgeon to manipulate tissues with minimal resulting damage. In addition, surgical simulator design can be improved to reflect more realistic tissue responses and evaluate trainees' tissue handling skills.

KEY WORDS—grasping, tissue damage, histological quantification, minimally invasive surgery, finite element analysis, surgical grasper

1. Introduction

Minimally invasive surgery (MIS), both traditional and robot-assisted, provides a number of patient benefits including re-

The International Journal of Robotics Research
Vol. 26, No. 11–12, November/December 2007, pp. 1159–1171
DOI: 10.1177/0278364907082847

Figures 1–6, 12, 13 appear in color online: http://ijr.sagepub.com

duced incidence of infection, shorter hospital stays and less pain (Yuen et al. 1998; Miyake et al. 2002). One current concern, however, is the lack of force feedback or haptic (touch) sensation available to the surgeon for safe tissue manipulation, making it possible for a surgeon to cause tissue damage by inadvertently applying excessive stress to tissue (Bethea et al. 2004; Bodner et al. 2004). Surgical simulators, which can be used to help train surgeons in MIS techniques, may not necessarily include force feedback and do not realistically portray tissues during manipulation (Thurfjell et al. 2001). Therefore, even during training, surgeons may not get a true sense of safe tissue handling.

1.1. Grasper induced damage

While there have been studies on complications and surgical stress due to surgical procedures at a macroscopic level (Yuen et al. 1998; Miyake et al. 2002), there is limited knowledge of localized short- and long-term effects of mechanical stresses due to tissue manipulation. Mechanical stress can cause unintentional injury to tissue by several means. One type of stress that might result in injury occurs during grasping for elevation, exposure or manipulation purposes, maneuvers that may result in crushing of tissue. By identifying stress magnitudes and durations that cause significantly increased tissue damage but are also within the range of those typically applied in MIS, it may be possible to create 'smart' surgical instruments that can guide a surgeon to manipulate tissues with minimal resulting damage. In addition, surgical simulator design would also be improved with more realistic tissue responses that would permit more accurate assessment of trainees' tissue handling skills.

1.2. Clinical relevance

Tissue damage during tissue manipulations can occur during robot-assisted or traditional MIS. There is evidence that laparoscopic cholecystectomies have a higher rate of damage to common bile duct, bowel and vascular structures compared to open surgery (Fletcher et al. 1999). Stress injury from graspers may result in pathological scar tissue formation, bleeding, adhesions and loss of bowel motility (Kalff et al. 1998, 1999; Anup and Balasubramanian 2000). Organs manipulated during MIS that may be injured in this way include liver, small bowel and ureter. All three are susceptible to severe grasping injuries including perforation or hemorrhage (Marucci et al. 2000; Heijnsdijk, Dankelman and Gouma 2002). However, even less severe immediate injury from grasping or manipulation may still result in clinically relevant consequences such as ileus (paralysis of the bowel), increased infection due to local breach of the bowel's protective barrier and increased adhesion formation (Reissman et al. 1996; Anup and Balasubramanian 2000).

Manipulations during gynecological procedures have up to a 1.5% rate of injury to the ureter, the consequences of which can include blockage, fistula formation and necrosis (Harkki-Siren et al. 1998; Ghali et al. 1999; Sakellariou et al. 2002). These effects may occur in a delayed fashion from interruption to the blood supply (ischemia), crushing of intracellular structures or bursting of cells. Secondary consequences such as inflammation, coagulation, cellular death and ischemia-reperfusion injury may follow and exacerbate this damage (Donati et al. 1998; Cotran et al. 1999; Shi and Pryor 2002; Ceylan et al. 2003).

1.3. Tissue response to injury

Three major aspects of tissue's acute response to injury include cellular changes, inflammation, and the consequences of vascular damage. The most severe cellular effects include apoptosis and necrosis, both forms of cell death. Inflammation is marked by infiltration of white blood cells (neutrophils, macrophages, and lymphocytes) and the respective chemical mediators that may be released. Vascular damage may include hemorrhage and activation of the multi-step coagulation cascade that ultimately results in the deposition of cross-linked fibrin (Cotran et al. 1999). Each of these three components of injury involves a large number of intermediate steps, including enzymatic activity, cellular responses, and chemical mediators that can be used to quantify the severity of injury.

1.4. Damage measurement

Little current data is available to suggest stress magnitudes and durations that are safe for tissue manipulation (De et al. 2006). Most previous studies have been qualitative in nature. For example, Elkins et al. (1987) evaluated the local injury to rabbit peritoneum from basic surgical maneuvers such as suture placement, excision and blunt abrasion. Injury sites were examined for acute markers of damage using histological staining, specifically hematoxylin and eosin or Masson-trichrome. White blood cell infiltrate, necrosis, fibrin deposition and collagen formation were correlated with survival studies that suggested adhesion formation was correlated with increased inflammation and necrosis (Elkins et al. 1987). This observation suggested that acute markers of tissue injury could be useful in predicting long-term consequences (Elkins et al. 1987; Ar'Rajab et al. 1996; Donati et al. 1998).

Studies specifically relating to tissue crush injury during grasping have also been qualitative. For example, Marucci et al. (2000) examined grasper trauma to the human gall bladder wall during laparoscopic cholecystectomies by analyzing epithelial loss, interstitial hemorrhage, and focal thinning of the wall. They found that increased grasp duration resulted in increased tissue damage.

Although not directly related to MIS, other studies of a more quantitative nature have been carried out on the effects of handling tissues during open surgery. Simmy et al. have quantified cellular, subcellular, and biochemical changes to rodent small bowel after manipulation, including cell viability and mitochondrial function (Simmy et al. 2001; 2005). In another study, Klaff et al. (1998) measured cellular infiltrates and changes in bowel muscularis function in rats from surgical manipulation. Their results indicated that gut paralysis correlated to the degree of trauma and the resulting inflammatory response. Neither study quantified the severity of the compressions applied to the bowel.

1.5. Need for finite element analysis

One difficulty in using a grasper to determine relationships between tissue damage and stress is that the stress distribution within a solid tissue that is being compressed is not uniform. The cross-sectional area of the grasper surface and the measured grasping force can be used to calculate the average nominal stress applied to the tissue by the grasper. This average stress does not provide any insight regarding the stress distribution and actual stress applied on individual cells between the grasper jaws. It is expected that there will be a uniform stress region between the grasper jaws with stress concentrations where the grasper edges contact the tissue surface. This area of uniform stress can be used to predict a physiological damage response to stress without the added confounding from damage observed at the stress concentrations. However, the size and shape of this uniform stress region is not known. While placing sensors in the tissue is one method of resolving this, tissue sensors may introduce further complexity due to tissue damage and alteration of tissue characteristics. Alternatively, computational modeling, such as finite element analysis, incorporates geometric and material properties to determine the local stress distributions within the tissue under compression. One example of this method has been demonstrated by Gunter et al. who used finite element modeling of vocal cords to better understand the distributions of stresses and possible related pathologies from high stresses during phonation (Gunter 2003).

1.6. Study design

In the present study, we sought to validate protocols to measure *in vivo* tissue damage as a function of the degree and duration of mechanical stress. The eventual goal of this work is to define stress levels that could be considered safe when applied to tissues in the course of routine MIS. As in the previous studies, many markers of coagulation, inflammation and cell death can serve as localized indicators of injury. The relative abundance of such markers can be measured and used to assess the degree of tissue trauma. Our research group has previously recorded characteristics of surgeons' movements during animal MIS procedures using a custom-built device named the Blue Dragon. These included magnitudes and durations of applied forces and torques at the surgeon-MIS instrument interface (Rosen et al. 2002; Brown 2003; Brown et al. 2004). For example, it was found that the mean grasp force applied was 8.52 ± 2.77 N and the mean 95% grasp time was 8.9 s.

In the present study, we were able to utilize these data to apply stress magnitudes and durations that are typically applied during MIS to porcine organs. A subset of these parameters was used to compute stress distributions in liver tissue between the grasper jaws using finite element analysis. These distributions were then used to guide the analysis of damage in the histological sections taken from the tissues stressed *in vivo*.

2. Methods

2.1. Grasping device

The motorized endoscopic grasper (MEG) is a second-generation computer-controlled device developed in the BioRobotics Laboratory for soft tissue testing (Brown et al. 2002; Brown 2003). Similar devices with various configurations and sensor capabilities have been constructed by other groups to measure tissue material properties for haptics and simulation (Bicchi et al. 1996; Ottensmeyer and Salisbury 2001; Tholey et al. 2004). The MEG is fitted with a Babcock-type (flat, paddle-like atraumatic) surgical grasper. Figure 1 shows a CAD drawing of the MEG and photographs of the Babcock grasper end effector and mechanism. The proximal end of the grasper tool is a ball joint that is connected to a partial pulley and cable. The motor in the handle of the MEG is attached to a capstan that drives the cable and pulley mechanism. The rotation of the motor is converted to a linear translation of the grasper shaft at the ball joint, actuating the grasper jaws to open and close. Force sensors (FR1010, 40 lb, Futek) in a two parallel beam full bridge strain gage configuration are mounted into the partial pulley to measure applied forces on the grasper's push/pull rod. An encoder, also attached to the motor, records the position of the grasper jaws.

The maximum force that can be applied by the MEG is 24.5 N, which is well beyond the requirements of this study. The MEG was calibrated using springs with known spring constants and silicone samples that simulated soft tissues. Current applied to the motor was correlated with the resulting force applied by the grasper jaws and the force measured by the force sensors. These experiments produced a relationship between input current and theoretical grasper force (Brown 2003):

$$I = \sigma \times \frac{G_A}{40} \tag{1}$$

where I is current (Amps), σ is measured in N m^{-2}, $G_A = 5.64 \times 10^{-5}$ m^2 represents grasper area and the constant on

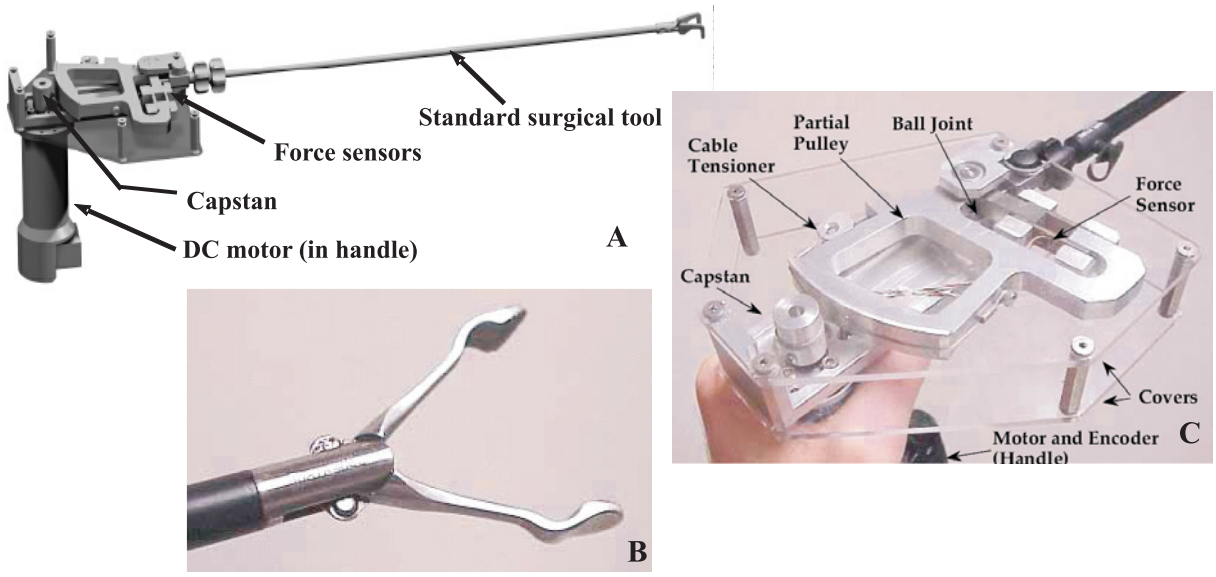

Fig. 1. (a) CAD drawing of the MEG; (b) close-up of MEG's Babcock grasper end effector and (c) MEG mechanism.

the denominator is measured in N Amp^{-1}. Sigma (σ) indicates stress and epsilon (ε) indicates strain.

Desired stresses were controlled via the current applied to the motor. The actual applied forces were measured with the strain gage recordings. The measured forces and calculated stresses were used for data analysis. Some error was expected between the theoretical and measured forces due to inherent friction in the tool mechanism. Routine calibrations between measured and actual force (using spring-based methods described above) suggest errors were typically well below 5%.

2.2. Animal experiments

This paper reports the results of repeated trials and multiple samples during a single animal experiment, which was conducted at the Center for Videoendoscopic Surgery under the University of Washington IACUC protocol #2469-04. The porcine model was chosen for this study as it is used for MIS training purposes and is commonly used as a model for human abdominal and pelvic organs (Heijnsdijk et al. 2002). On the day of the experiment, an adult female farm pig (~30 kg) was placed under full IV and inhalation anesthesia by a veterinary technician. A laparotomy was performed to expose the organs. The MEG was used to apply compression stresses, between 0–240 kPa (theoretical values of 0, 60, 120, 180 and 240 kPa) at regular intervals along the liver edge, small bowel jejunum and ureter. Figure 2a shows cross-sectional schematic diagrams of grasping during the experiments. Based on visual and microscopic examination of the grasped sites, the arms of the graspers did not make any significant contact with the tissues. Actual forces applied by the grasper were measured by the MEG and recorded along with the tissue deformations (based on encoder readings).

All results are measured, not theoretical, force or stress unless otherwise noted, with a control of 0 kPa consisting of the jaws just touching the tissue surface. Compression stresses were held for 10 or 30 s. These parameters were based on previously collected data from the Blue Dragon experiments on surgical movements in MIS. Each set of parameters was repeated at least three times (i.e. 60 kPa for 10 s on liver is repeated three times, each at a different site). Figures 2b–d show small bowel, ureter, and liver during *in vivo* experimentation. The injury response was allowed to develop for three hours at which time the animal was euthanized and the tissues were harvested and fixed for histology.

2.3. Histology

Tissue processing and staining was carried out at the clinical and research histology laboratories at the Department of Pathology, University of Washington. Tissues were fixed in 10% buffered formalin and embedded in paraffin. Standard 5-micrometer paraffin sections were mounted on glass. Multiple sections were taken from each crushed tissue sample parallel to the direction of applied compressive stress. Each section was stained once for a particular measure of interest. For initial examination, sections were stained with hematoxylin and eosin (H&E) for visualization of overall changes in morphology and architecture, as well as cellular death, which is marked either by increased cytoplasmic eosinophilia (intensity of red/pink stain) with nuclear pyknosis (condensed, hyperchromatic nucleus), or by overt apoptosis with nuclear fragmentation.

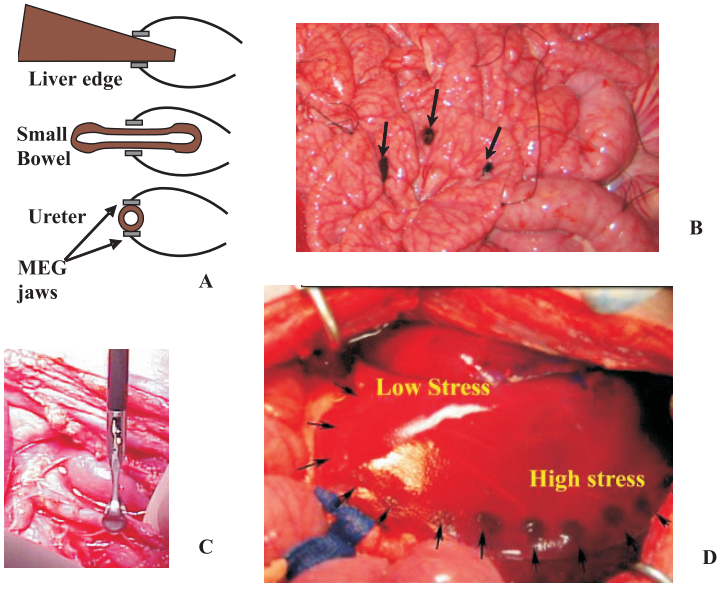

Fig. 2. (a) Schematic diagrams of the tissue grasper cross-section during *in vivo* stress application. (b) *In vivo* image of small bowel after three stress applications. Sutures and ink (arrows) mark crush sites since no clear visual change is apparent at tissue harvesting. (c) *In vivo* image of MEG applying stress to ureter. (d) *In vivo* image of liver with multiple compression sites (arrows). Lower stresses (60 kPa) begin at upper left with increasing stress magnitudes up to the highest stresses (240 kPa) at lower right.

Figure 3 shows examples of H&E stained tissues. Figure 3A demonstrates injury to the small bowel mucosa with a clear breach of the small bowel protective barrier. Figures 3b–d show changes in liver architecture and cellular morphology with increases in stress magnitude.

2.4. Inflammation

Neutrophils were stained for myeloperoxidase (MPO) using polyclonal antibody (DakoCytomation) immunohistochemistry (IHC) (Pinkus and Pinkus 1991). All IHC analyses used a standard avidin-biotin-peroxidase complex (ABC) technique (Hsu et al. 1985) following microwave-based epitope retrieval in 0.01 M citrate buffer (pH 6.0). 3.3'-diaminobenzidine 4HCl (DAB) was used as the chromogen and slides were counterstained with Harris hematoxylin (blue). Figure 4 shows ureter (control and 180 kPa, 30 s grasps) with neutrophils demonstrating a cytoplasm-based anti-MPO reaction (neutrophils appear brown from the brown DAB precipitate, as highlighted by arrows).

2.5. Apoptosis

Activated caspase-3 antibody (polyclonal antibody, Cell Signaling Technologies) IHC was used to quantify apoptotic cell death with a methodology (including epitope retrieval) that

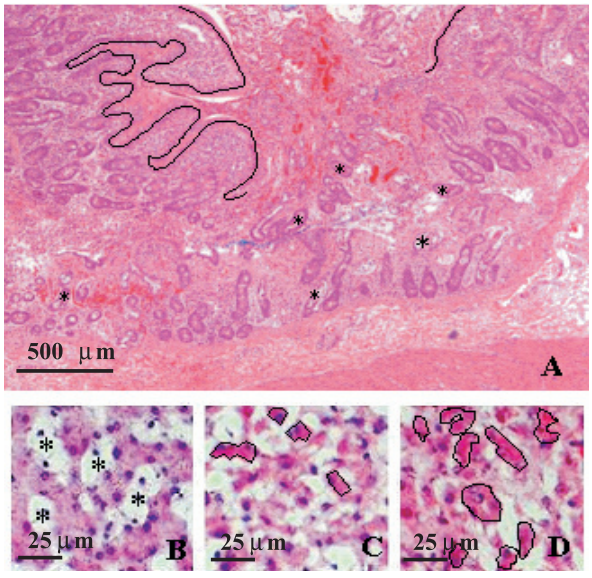

Fig. 3. H&E stain, 10 second grasp for (a) small bowel and (b–d) liver. (a) Cross-section with lumen at the top, 220 kPa. Clear destruction of villi, abnormal crypts (*), break in line indicates break in endothelial barrier. (b) Control (0 kPa), normal hepatocytes and sinusoids (*); (c) 100 kPa, contracted cells and eosinophilia (outlined) with some normal hepatocytes; and (d) 200 kPa, increased eosinophilia (outlined), abnormal nuclei and loss of sinusoids.

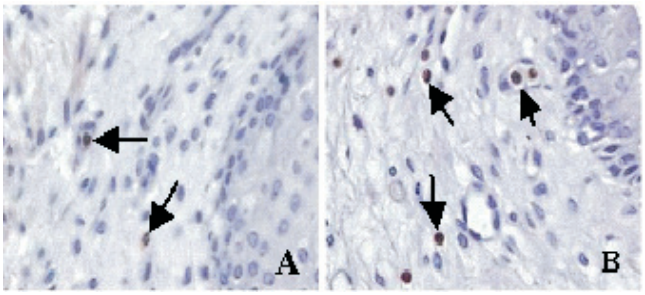

Fig. 4. Highly magnified ureter. Myeloperoxidase IHC for neutrophils, (a) control and (b) 180 kPa. Arrows indicate neutrophils (which stain brown).

was identical to that employed for myeloperoxidase (Gown and Willingham 2002). Figures 5a and 5b show apoptosis in small bowel (brown DAB precipitate in the cytoplasm and nuclear fragments of positive cells, as highlighted by arrows) in control (0 kPa) and injured tissue (251 kPa), respectively. Note that all results are given based on measured stress unless otherwise indicated.

2.6. Quantification and image analysis

Multiple images within the crush site were taken from several sections of each injury site at 400X. The images were taken from the center of the crush injury site. Based on engineering principles and the finite element analysis described below, the center region between the grasper jaws is most representative of the average measured stress. Neutrophils were manually counted within a field of view. Apoptotic cells were measured using Image J and image analysis software available through the NIH website (http://rsb.info.nih.gov/ij/). Image analysis was used to determine percent area of apoptotic cells in a field of view as apoptotic cells ultimately fragment and cannot be counted. Quantification was based on the total number of pixels (i.e. area) within a field of view that was marked by the respective antibody. The background was subtracted from the original image and then split into its RGB components. A manually identified threshold that most completely identified the apoptotic stained cells was applied to the blue channel and the percent area of staining was determined. The same threshold was used for all images taken from a single slide.

Figure 5 displays results of IHC and image analysis for identifying and quantifying labeled cells within the crush area. Figure 5a (zero applied stress) illustrates normal cell turnover (apoptotic cells are brown). Figure 5b is of crushed small bowel (251 kPa) with an increase in apoptotic cells. Figures 5c and 5d show the blue channel of Figures 5a and 5b, respectively, after background removal and RGB split. Figures 5e

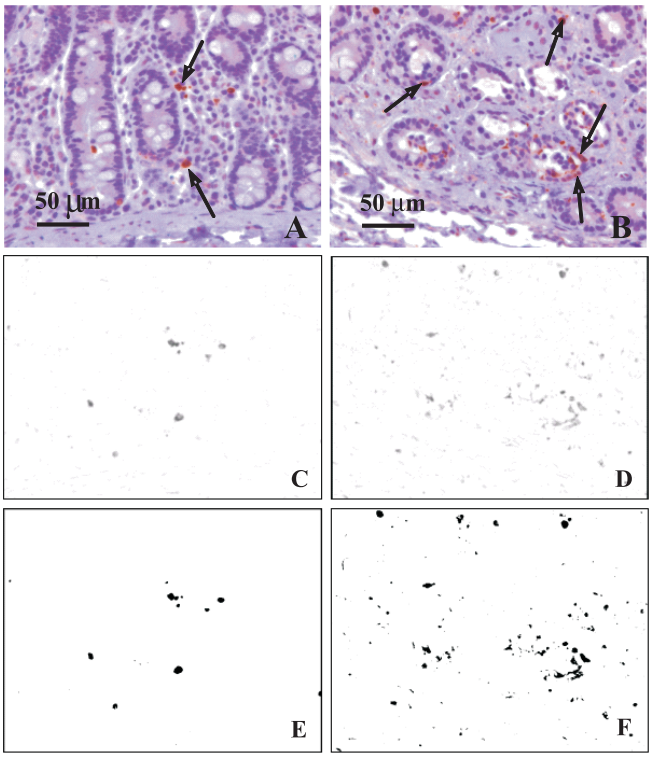

Fig. 5. Small bowel mucosa at a magnification of 400X. (a) and (b) Control and 251 kPa (10 s), respectively. Caspase-3 IHC original images; arrows indicate apoptotic cells (which stain brown). (c) and (d) Blue channels of (a) and (b) after background subtraction and RGB split. (e) and (f) Final post-threshold images of (a) and (b).

(percent stained = 0.38%) and 5F (percent stained = 1.51%) show the final post-threshold images of 5a and 5b, respectively, where black represents the apoptotic cells originally stained brown. Between nine and twelve total images at 400X magnification were collected from three different crush sites for each set of stress parameters analyzed and reported here.

For each image analysis technique used, either manually counting cells or setting thresholds, inter-observer variability was negligible (1–5%). Inter-observer variability was generally not noted since the same individual performed all analysis.

2.7. Finite element analysis

Finite element analysis (FEA) was carried out for two-dimensional models of liver, simulating the sections of liver used for histology. Two different models were created in ANSYS, each with certain assumptions. First, a model was built with similar geometrical dimensions as the triangular histological liver sections (the apex represented the free edge of the

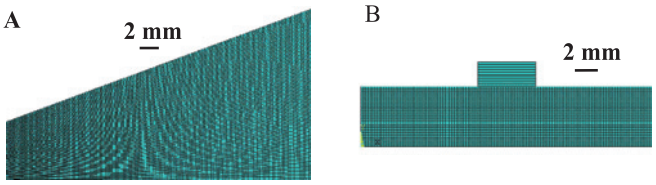

Fig. 6. Mesh of liver model with (a) geometric fidelity and linear tissue properties and (b) using nonlinear tissue properties and symmetry. The small upper block represents the grasper jaw and the large rectangle represents the liver.

liver and the base represented the thicker, central portion of the liver). Boundary conditions included fixing the base displacement (representing the remaining 'infinitely' large liver) in the x- and y- directions. The tissue model was given isotropic, homogeneous, linear elastic properties (Brown 2003; Brown et al. 2003). Young's modulus was set a value of 150 kPa and Poisson's ratio was set at 0.45, since liver tissue is almost incompressible.

The mesh for this model (Figure 6a) consisted of 4-node quadrilateral elements. To simulate grasping at a level of 240 kPa, a corresponding experimentally-measured strain of 0.4 was applied to the top and bottom of the tissue model (note that the expected stress will be 60 kPa due to the linear stiffness). The von Mises stress distribution of the static analysis was displayed.

The second FEA was built utilizing non-linear material properties, but a simplified geometry. This model took advantage of symmetry in the system, such that only half of the tissue and one grasper jaw were modeled and analyzed. The tissue was represented by a large rectangle and a smaller rectangle above the tissue represented the grasper jaw. Boundary conditions were based on symmetry so that the horizontal plane of symmetry, not touching the grasper, was fixed in the y-direction and only a few center nodes were fixed in the x-direction (since the tissue can horizontally translate). In this computation, the tissue had non-linear tissue properties based on a stress-strain tissue model (Equation 2) that was previously studied experimentally by Brown (2003). The model used here is of the form

$$\sigma = \mathrm{A}(e^{\mathrm{B}\varepsilon^2} - 1) + \mathrm{C}\varepsilon. \quad (2)$$

In the original model, the constants A, B and C were set at 7377, 21 and 3289, respectively. However, uniaxial stress and strain had very low stiffness in the initial low stress region, causing the iterative process in ANSYS to produce errors. Therefore, the value of the constant C was altered to C = 100 000 to increase the stiffness in the 'toe' region, allowing the iterative solver to complete.

This alteration did not greatly change the overall non-linear tissue property. Data points were generated using the stiffer model and an order 1 Ogden model was fit by ANSYS to be

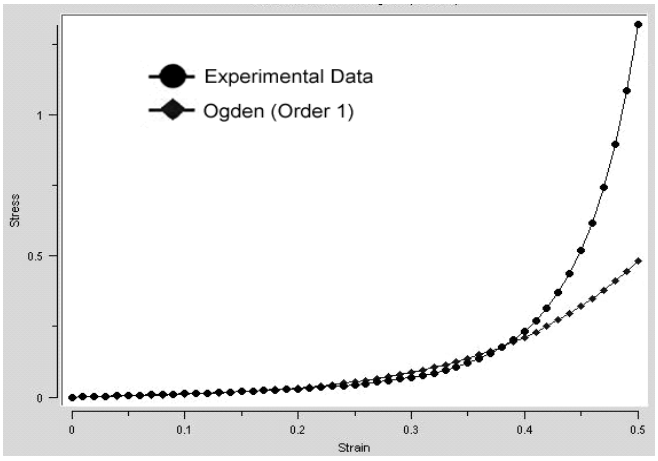

Fig. 7. Altered, stiffer tissue model (Exp Data 1) and calculated Ogden fit (Ogden order 1).

used in the FE solution. A plot of the fit model is shown in Figure 7. The Ogden model fits the data points well within the region of interest (strain ≤ 0.4). The grasper was given material properties of surgical steel 316 (E = 190 GPa, v = 0.27). E is Young's modulus and v is Poisson's ratio. The mesh for this model, seen in Figure 6b, consisted of 4-node quadrilateral elements of the same size as the previous model. Special contact elements had to be created at the contact surface for the grasper to push on the tissue. Again, a strain of 0.4 (measured experimentally during stress application of 240 kPa) was applied by the modeled grasper. Output was plotted as principle stress, von Mises stress and displacement.

The general contours or stress distributions were used to guide the analysis of the histological sections. Only damaged areas within the central region of uniform stress were included in the measurement of tissue damage parameters.

2.8. Statistics

ANOVA analyses were completed for each organ and tissue damage parameter pair (i.e. liver, apoptosis) with the independent variable being stress magnitude or duration. If the p-value of the ANOVA indicated a significant difference (i.e. $p < 0.05$), then Bonferroni multiple comparison tests were performed. A p-value equal to or less than 0.05 was considered significant for the multiple comparison tests.

3. Preliminary Results

Stress application with the MEG was repeatable with low variance. Horizontal error bars indicate standard deviation of applied stress, which was less than 6% of applied stress magnitude for all conditions (Figures 8–11).

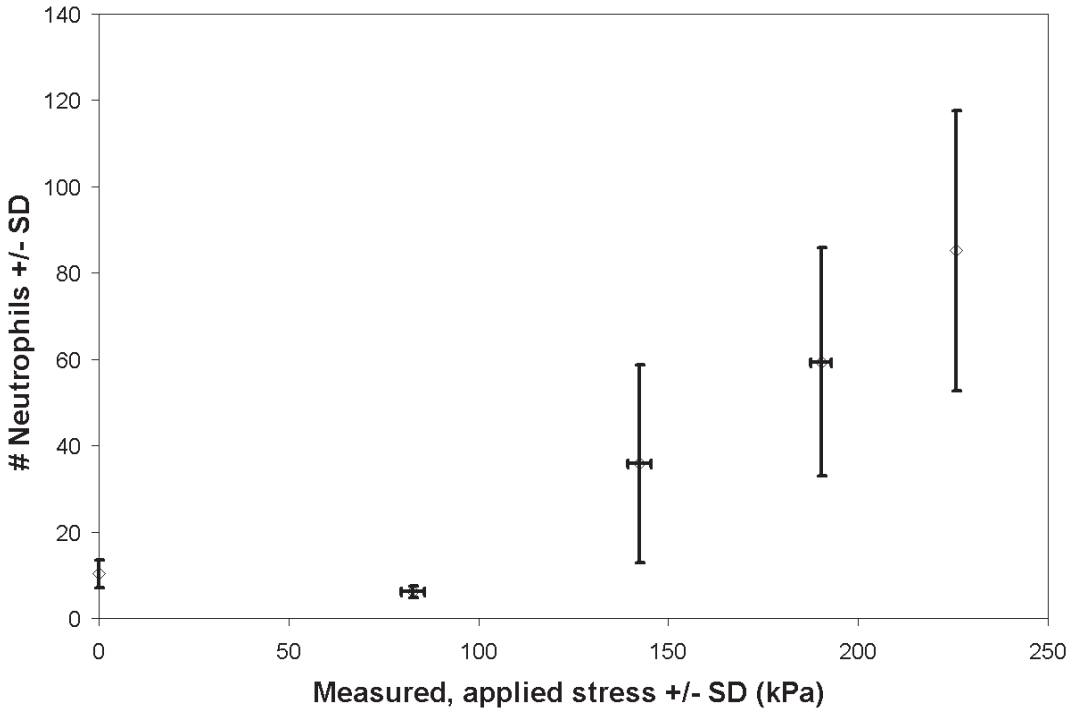

Fig. 8. Number of neutrophils versus applied stress magnitude for the small bowel, 30 second grasps.

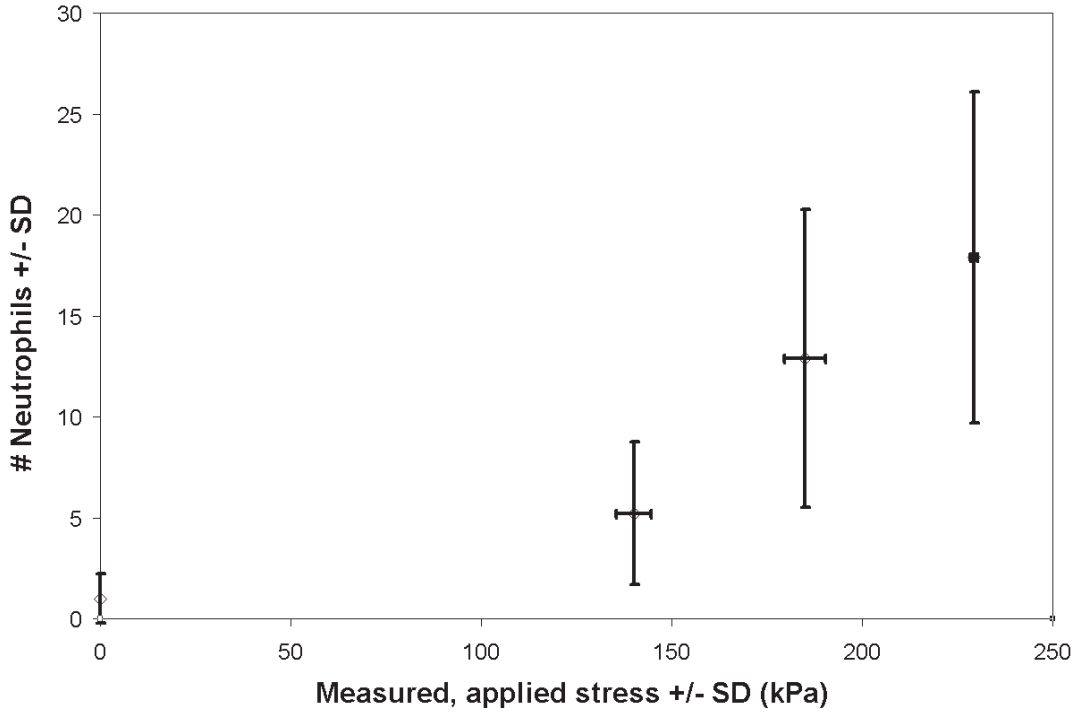

Fig. 9. Number of neutrophils versus applied stress magnitude for the ureter, 30 second grasps.

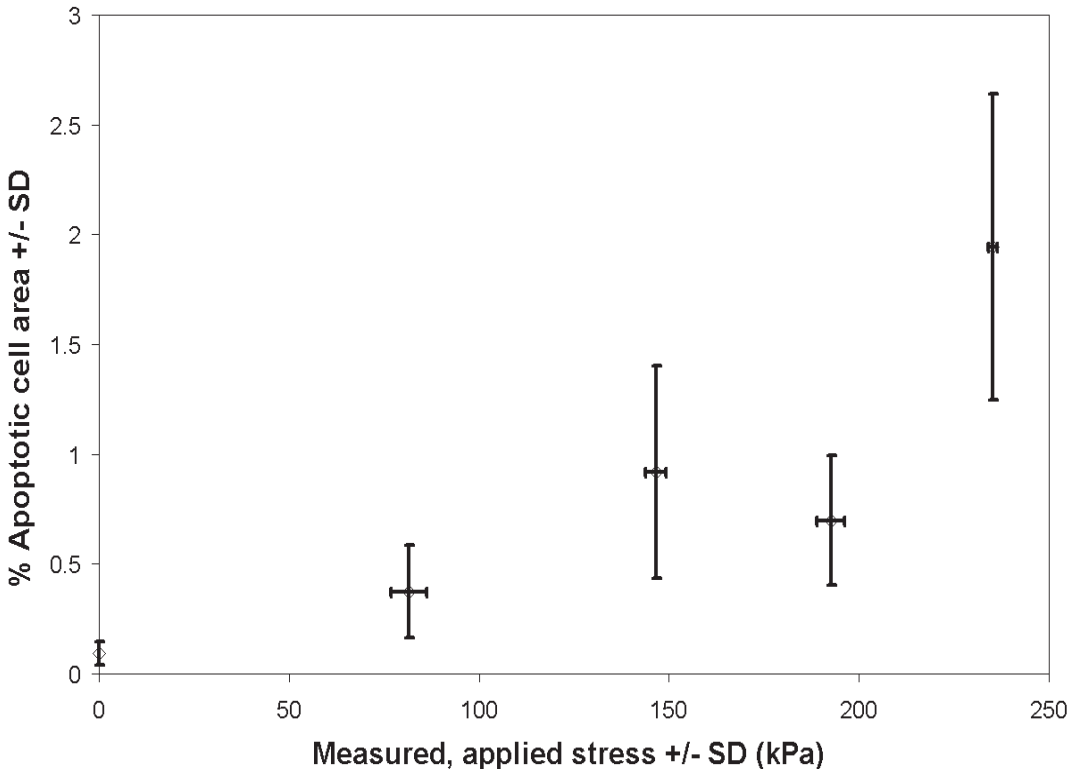

Fig. 10. Percent apoptotic labeled cell area versus applied stress magnitude for the liver, 30 second grasps.

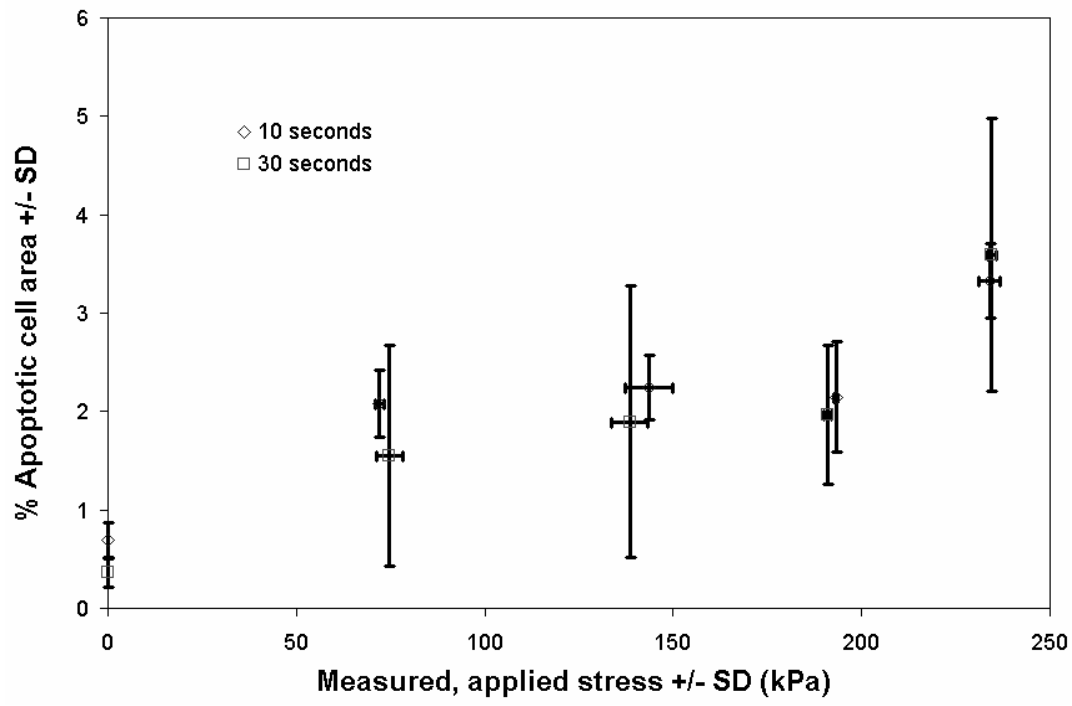

Fig. 11. Percent apoptotic labeled cell area versus applied stress for the small bowel, 10 and 30 second grasps.

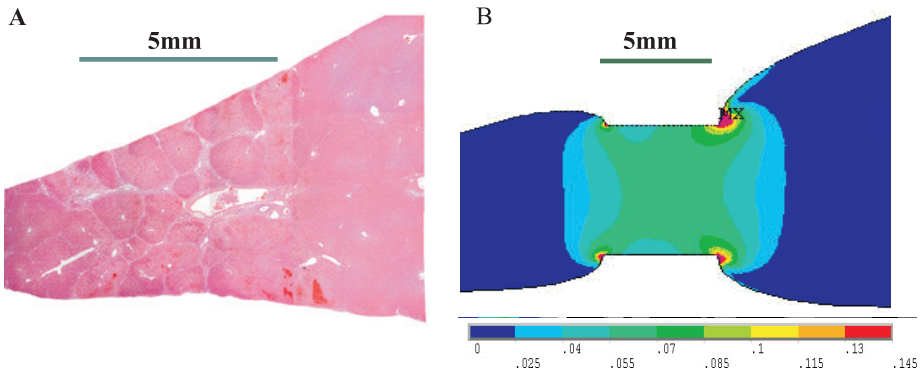

Fig. 12. (a) H&E section of liver with an applied vertical compression. Bar indicates width of contact with grasper jaws. (b) Close-up of von Mises stress plot of FEA using linear material properties. Scale is in MPa. MX marks the region of maximum stress.

3.1. Neutrophils

The number of neutrophils increased with stress magnitude in the small bowel after 30 second grasps (Figure 8). Statistical analyses indicated a significant difference (i.e. the multiple comparison p-value < 0.05) between the control group and both the 180 kPa and 240 kPa groups. Similar results were seen for the ureter. In Figure 9, note that there is a missing stress group for ureter ($\sim$60 kPa). This is due to the fact that there was limited ureter tissue available for testing.

3.2. Apoptosis

In liver subjected to 30 second grasps, percent apoptotic labeled pixels increased with stress magnitude (Figure 10). ANOVA analyses followed by multiple comparison tests indicated that there was significantly increased apoptosis with 180 kPa and 240 kPa compared to the control. Again, percent apoptotic labeled pixels increased with stress magnitude for both 10 and 30 second grasps in the small bowel (Figure 11). There was no significant difference between the responses with respect to grasp duration. For the 10 second grasp, 240 kPa resulted in significantly greater apoptosis compared to all other stress groups. There was also a significant difference between 240 kPa and the control with a 30 second grasp.

A small increase in apoptosis with increasing stress magnitude was observed in the ureter, but the difference between stress groups was not significant.

3.3. Finite element analysis

FEA assumptions were more applicable in liver due to the homogeneous nature of the tissue. The first FEA model using linear elastic tissue model can be validated by the linear stress–strain relationship $\sigma = E\varepsilon$. Validation is required to assure that model inputs produce logical outputs. Based on the assigned linear properties and an input strain of 0.4, the predicted average stress of approximately 60 kPa was observed. This model, which used the linear tissue property assumptions but more accurate geometry, produced results that could be directly compared to the histological sections, as in Figures 12a and 12b. Figure 12a shows an H&E stained section of liver that was vertically compressed by the MEG. Figure 12b shows the von Mises stress calculated for the analogous FEA model with an applied strain of 0.4 (equivalent to the experimental 240 kPa stress application). In comparing the FEA model to the histological section, it can be seen that the sites of stress concentration correspond to the sites of increased vascular damage (evidenced by red blood clots) in the tissue.

The FEA model utilizing symmetry, contact with the grasper and non-linear tissue properties predicted similar von Mises stress contours (disregarding the different geometry) as the linear elastic model, although actual values were different (Figure 13a). The model was verified, as there was less than 5% error between the predicted average stress and the experimentally measured average stress of 240 kPa corresponding to a strain of 0.4. Figure 13b shows a plot of the principal stresses for this model. As expected, the principal axis aligned with the y axis in the majority of the cross-section with high stress concentrations in the corners. Note that both plots 13a and 13b represent zoomed-in images of the compression site.

Stress distributions in both models show the size of the central region with the more uniform stress distribution. Tissue damage was measured, as described above, in these regions.

4. Discussion and Conclusions

Identification of stress magnitudes and durations that cause minimal trauma to patient organs during manipulation may

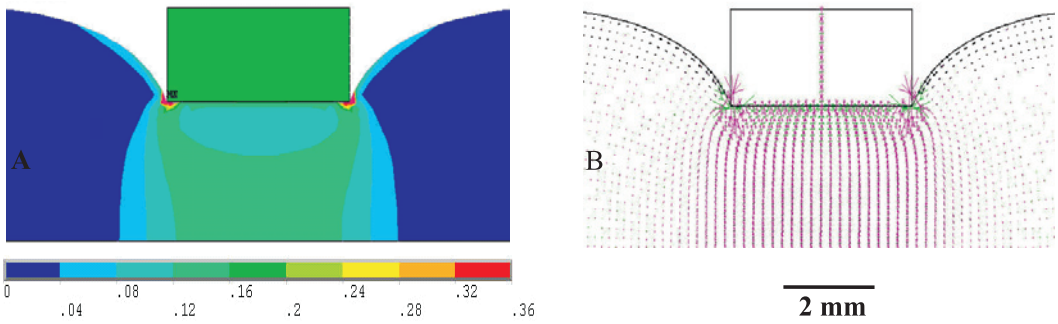

Fig. 13. (a) Close-up of von Mises stress plot of FEA using nonlinear material properties. Scale is in MPa. (b) Close-up of vector plot of principle stresses (black = σ_1, green/light gray = σ_2, pink/dark gray = σ_3). Length is proportional to stress magnitude.

help alleviate pain and avoid potentially significant consequences in MIS by helping guide a surgeon to safely manipulate tissues. Surgical tools could be equipped with alarms or lights to indicate application of excessive stresses (Kitagawa et al. 2005). In addition, surgical simulators may be improved by having more realistic tissue responses as well as feedback regarding trainees' handling of tissues. In order to identify such stress thresholds and stress dose responses, we must first determine an appropriate methodology that will include quantitative techniques to measure both the stresses applied and the resultant tissue damage.

In this study, we used a device that was specifically designed to apply known stresses to tissues *in vivo*, providing quantitative data on stress duration and magnitude. Using this device, stresses within the range of those typically applied during MIS were applied to several types of tissues and measured. Based on our preliminary results, the MEG is an appropriate tool for our purposes. Desired stresses were applied and measured with minimal standard deviations within each group.

Finite element models were created to better understand the stress distributions within the tissues during compressions. The model with greater geometric fidelity demonstrated that localized stress concentrations were found in similar regions as local areas of qualitatively-assessed increased damage to tissue sections. The model with more complex tissue properties and contact with a grasper showed expected stress distributions. Both models suggested that to fairly assess tissue damage between different specimens, the location of assessment should be consistent. In this case, the central region of the compression zone was chosen because it was easily identifiable and consistently showed a more uniform stress level.

These FE models were preliminary in nature in that several assumptions and simplifications were made. Again, the purpose of these models was to provide a guide for histological analysis such that the measured average stress is predictive of a particular physiological response; however, it is our aim to generate more accurate models. We plan to combine the geometric fidelity with the nonlinear tissue properties as well as add adaptivity to the high stress regions of the mesh. We will also incorporate tissue anisotropy as more data regarding tissue properties become available (Hollenstein et al. 2006; Chui et al. 2007).

It is important to note that no model will be highly accurate, as all the relevant material and geometric properties do not currently exist. In addition, these models are meant to mimic the *in vivo* experiments; control of boundary conditions while using surgical instruments is extremely difficult to achieve without potentially altering tissue physiology. While the FEA was only carried out for models of liver for this preliminary study, a similar result is expected in other tissues, although with different predicted values. Models with greater accuracy for liver and other organs will be created in the future and could have additional applications, such as grasper shape or design testing. However, the current models serve as an initial basic guide for identifying the area for damage analysis in all tissues.

To assess the tissue damage resulting from compression stresses, we used histology for measuring cellular death and inflammation, with plans to also measure activation of the coagulation cascade. Our preliminary data showed a dose-dependent response to stress magnitude as indicated by apoptosis in all three tissues and neutrophil infiltration in small bowel and ureter. Qualitative assessment of H&E stained sections of small bowel and liver showed increased areas of coagulation (clot formation) with increasing stress magnitude. No obvious differences in coagulation from different stress magnitudes were observed in the ureter. Based on these preliminary results, it is possible that a threshold may exist around 180 kPa of compression stress for the tested tissues, but clearly additional animals must be tested.

ANOVA analysis indicated statistically significant differences in tissue damage between stress magnitudes in multiple tissues and with multiple measures of injury. Although these results must be viewed with caution as they derive from multiple samples within one study animal, the data suggest that the histological methods selected were sensitive enough to distinguish between varying levels of injury within our range of

interest in liver and small bowel. Statistically significant differences were seen with inflammation, but not cellular death, in the ureter. However, this may be representative of this tissue's response rather than the sensitivity of our assays. It is possible that because the ureter contains a higher proportion of connective tissue and muscle as compared to the liver and to some degree small bowel, the ureter may not have as great an injury response demonstrated by cellular death and coagulation, although it still exhibits inflammation.

The last step in finalizing our methodology will involve analysis of the remaining sets of stress parameters, including measurement of inflammation in liver. We will include an additional stress duration of 60 seconds as suggested by the aforementioned Blue Dragon results, which is infrequent, but within the range of durations typically applied during surgery. An additional stress magnitude of 300 kPa will be tested to encompass the 99% confidence interval of mean grasping stress, with the exception of liver as this exceeds biomechanical failure (defined here as a drop in stress despite an increase in strain). We will also include a quantitative measure for fibrin to represent activation of the coagulation cascade. This will be carried out using IHC analyses with a monoclonal anti-fibrin antibody (Edgell *et al*. 1996), using the detection and image analysis methods described above. Immunoreactivity commensurate with fibrin deposition can be used as a marker of activation of the coagulation cascade.

Future research will be focused on identifying tissue damage thresholds and stress dose response curves for multiple organs with statistically significant sample sizes using this methodology.

Acknowledgements

This work is partially supported by the NIH (67-1450), NSF (66-6531), the Army (62-8360), the Center for Videoendoscopic Surgery and UW Department of Anatomic Pathology. We would like to thank the Center for Videoendoscopic Surgery and the Department of Anatomic Pathology at the University of Washington for the use of space, supplies and expertise. We would also like to acknowledge Dr Gaffney, Department of Surgery, St Thomas Hospital, London for the use of the fibrin antibody and members of the UW Biorobotics laboratory for their support.

References

Anup, R. and Balasubramanian, K. A. (2000). Surgical stress and the gastrointestinal tract. *Journal of Surgical Research*, **92**(2): 291–300.

Ar'Rajab, A. et al. (1996). The role of neutrophils in peritoneal adhesion formation. *Journal of Surgical Research*, **61**(1): 143–146.

Bethea, B. T. et al. (2004). Application of haptic feedback to robotic surgery. *Journal of Laparoendoscopic and Advanced Surgical Techniques*, **14**(3): 191–195.

Bicchi, A. et al. (1996). A sensor-based minimally invasive surgery tool for detecting tissue elastic properties. *Proceedings of IEEE International Conference on Robotics and Automation.* Minneapolis, USA, vol. 1, pp. 884–8.

Bodner, J., Wykgpiel, H., Wetscher, G., Schmid, T. (2004). First experiences with the da Vinci operating robot in thoracic surgery. *European Journal of Cardio-Thoracic Surgery*, **25**(5): 844–851.

Brown, J. D. (2003). In-Vivo and Postmortem Biomechanics of Abdominal Organs Under Compressive Loads: Experimental Approach in a Laparoscopic Surgery Setup. Ph.D. thesis, University of Washington, **85**: 71–3.

Brown, J. D. et al. (2002). Computer-controlled motorized endoscopic grasper for in vivo measurement of soft tissue biomechanical characteristics. *Studies in Health Technology and Informatics*, 8571–73.

Brown, J. D. et al. (2003). In-vivo and in-situ compressive properties of porcine abdominal soft tissues. *Studies in Health Technology and Informatics*, **94**: 26–32.

Brown, J. D. et al. (2004). Quantifying surgeon grasping mechanics in laparoscopy using the Blue DRAGON system. *Studies in Health Technology and Informatics*, **98**: 34–6.

Ceylan, H. et al. (2003). Temporary stretch of the testicular pedicle may damage the vas deferens and the testis. *Journal of Pediatric Surgery*, **38**(10): 1530–1533.

Chui, C. et al. (2007). Transversely isotropic properties of porcine liver tissue: experiments and constitutive modelling. *Medical & Biological Engineering & Computing*, **45**(1): 99–106.

Cotran, Kumar, V., Collins, T. (1999). Pathological Basis of Disease, Sixth edition. W. B. Saunders Company, Philadelphia, PA.

De, S. et al. (2006). Assessment of Tissue Damage due to Mechanical Stresses. *Proceedings of IEEE/RAS-EMBS International Conference on Biomedical Robotics and Biomechatronics*. Pisa, Italy, pp. 823–828.

Donati, A. et al. (1998). Predictive value of interleukin 6 (IL-6), interleukin 8 (IL-8) and gastric intramucosal pH (pH-i) in major abdominal surgery. *Intensive Care Medicine*, **24**(4): 329–335.

Edgell, T., McEroy, F., Webbon, P., Gattney, P. J. (1996). Monoclonal antibodies to human fibrin: interaction with other animal fibrins. *Journal of Thrombosis and Haemostasis*, **75**(4): 595–599.

Elkins, T. E. et al. (1987). A histologic evaluation of peritoneal injury and repair: implications for adhesion formation. *Journal of Obstetrics and Gynaecology*, **70**(2): 225–228.

Fletcher, D. R. et al. (1999). Complications of cholecystectomy: risks of the laparoscopic approach and protective

effects of operative cholangiography: a population-based study. *Annals of Surgery*, **229**(4): 449–457.

Ghali, A. M. et al. (1999). Ureteric injuries: diagnosis, management, and outcome. *Journal of Trauma*, **46**(1): 150–158.

Gown, A. M. and Willingham, M. C. (2002). Improved detection of apoptotic cells in archival paraffin sections: immunohistochemistry using antibodies to cleaved caspase. *Journal of Histochemistry and Cytochemistry*, **50**(4): 449–454.

Gunter, H. E. (2003). A mechanical model of vocal-fold collision with high spatial and temporal resolution. *Journal of Acoustical Society of America*, **113**(2): 994–1000.

Harkki-Siren, P., Sjoberg, J. and Tiitinen, A. (1998). Urinary tract injuries after hysterectomy. *Journal of Obstetrics and Gynecology*, **92**(1): 113–118.

Heijnsdijk, E. A., Dankelman, J. and Gouma, D. J. (2002). Effectiveness of grasping and duration of clamping using laparoscopic graspers. *Surgical Endoscopy*, **16**(9): 1329–1331.

Hollenstein, M. et al. (2006). Mechanical Characterization of the Liver Capsule and Parenchyma. Lecture Notes in Computer Science: Biomedical Simulation, pp. 150–158. Springer Berlin/Heidelberg.

Hsu, S. M., Yang, K. and Jaffe, E. S. (1985). Phenotypic expression of Hodgkin's and Reed-Sternberg cells in Hodgkin's disease. *American Journal of Pathology*, **118**(2): 209–217.

Kalff, J. C., Schraut, W. H., Simmons, R. L., Bauer, A. J. (1998). Surgical manipulation of the gut elicits an intestinal muscularis inflammatory response resulting in postsurgical ileus. *Annals of Surgery*, **228**(5): 652–663.

Kalff, J. C. et al. (1999). Surgically induced leukocytic infiltrates within the rat intestinal muscularis mediate postoperative ileus. *Gastroenterology*, **117**(2): 378–387.

Kitagawa, M., Dokko, D., Okamura, A. M., and Yuh, D. D. (2005). Effect of sensory substitution on suture-manipulation forces for robotic surgical systems. *Journal of Thorac and Cardiovascular Surgery*, **129**(1): 151–158.

Marucci, D. D. et al. (2000). Grasper trauma during laparoscopic cholecystectomy. *ANZ Journal of Surgery*, **70**(8): 578–581.

Miyake, H. et al. (2002). Comparison of surgical stress between laparoscopy and open surgery in the field of urology by measurement of humoral mediators. *International Journal of Urology*, **9**(6): 329–333.

Ottensmeyer, M. P. and Salisbury, J. K. (2001). In Vivo Data Acquisition Instrument for Solid Organ Mechanical Property Measurement. Lecture Notes in Computer Science: Medical Image Computing and Computer-Assisted Intervention, pp. 975–982. Springer Berlin/Heidelberg.

Pinkus, G. S. and Pinkus, J. L. (1991). Myeloperoxidase: a specific marker for myeloid cells in paraffin sections. *Modern Pathology*, **4**(6): 733–741.

Reissman, P. et al. (1996). Adhesion formation after laparoscopic anterior resection in a porcine model: a pilot study. *Surgical Laparoscopy and Endoscopy*, **6**(2): 136–139.

Rosen, J. et al. (2002). The Blue DRAGON: a system for monitoring the kinematics and the dynamics of endoscopic tools in minimally invasive surgery for objective laparoscopic skill assessment. *Studies in Health Technology and Informatics*, **85**: 412–418.

Sakellariou, P. et al. (2002). Management of ureteric injuries during gynecological operations: 10 years experience. *European Journal of Obstetics & Gynaecology Reproductive Biology*, **101**(2): 179–184.

Shi, R. and Pryor, J. D. (2002). Pathological changes of isolated spinal cord axons in response to mechanical stretch. *Neuroscience*, **110**(4): 765–777.

Simmy, T., Anup, R., Prabhu, R., Balasubramanian, K. A. (2001). Effect of surgical manipulation of the rat intestine on enterocyte populations. *Surgery*, **130**(3): 479–488.

Simmy, T., Prabhu, R. and Balasubramanian, K. A. (2005). Surgical manipulation of the intestine and distant organ damage-protection by oral glutamine supplementation. *Surgery*, **137**(1): 48–55.

Tholey, G. et al. (2004). Design, Development, and Testing of an Automated Laparoscopic Grasper with 3-D Force Measurement Capability. Lecture Notes in Computer Science: Medical Simulation, pp. 38–48. Springer Berlin/Heidelberg.

Thurfjell, L., Lundin, A. and McLaughlin, J. (2001). A medical platform for simulation of surgical procedures. *Studies in Health Technology and Informatics*, **81**: 509–514.

Yuen, P. M. et al. (1998). Metabolic and inflammatory responses after laparoscopic and abdominal hysterectomy. *American Journal of Obstetrics and Gynecology*, **179**(1): 1–5.